Supplementary Information

Facet-Dependent Adsorbate-Mediated Strong Metal-Support Interaction in Ni/TiO_2

Liboting Gao[1†], Hao Zhang[1,3†], Yanhui Long[1†], Fangwen Yang[2], Zijiang Zhao[1], Rui Tang[2], Yilin Zhang[1], Xiaosong An[1], Wentao Yuan[2*], Yong Wang[2*], Jianhua Yan[1,3*]*

[1]State Key Laboratory of Clean Energy Utilization, Zhejiang University, Hangzhou, 310027, China.
[2]Center of Electron Microscopy and State Key Laboratory of Silicon and Advanced Semiconductor Materials, School of Materials Science and Engineering, Zhejiang University, Hangzhou, 310027, China.
[3]Inner Mongolia Daqingshan Laboratory, Hohhot, 017000, China.
†These authors contributed equally to this work.

*Corresponding author.

Emails: zhang_hao@zju.edu.cn, wentao_yuan@zju.edu.cn; yongwang@zju.edu.cn; yanjh@zju.edu.cn

Contents

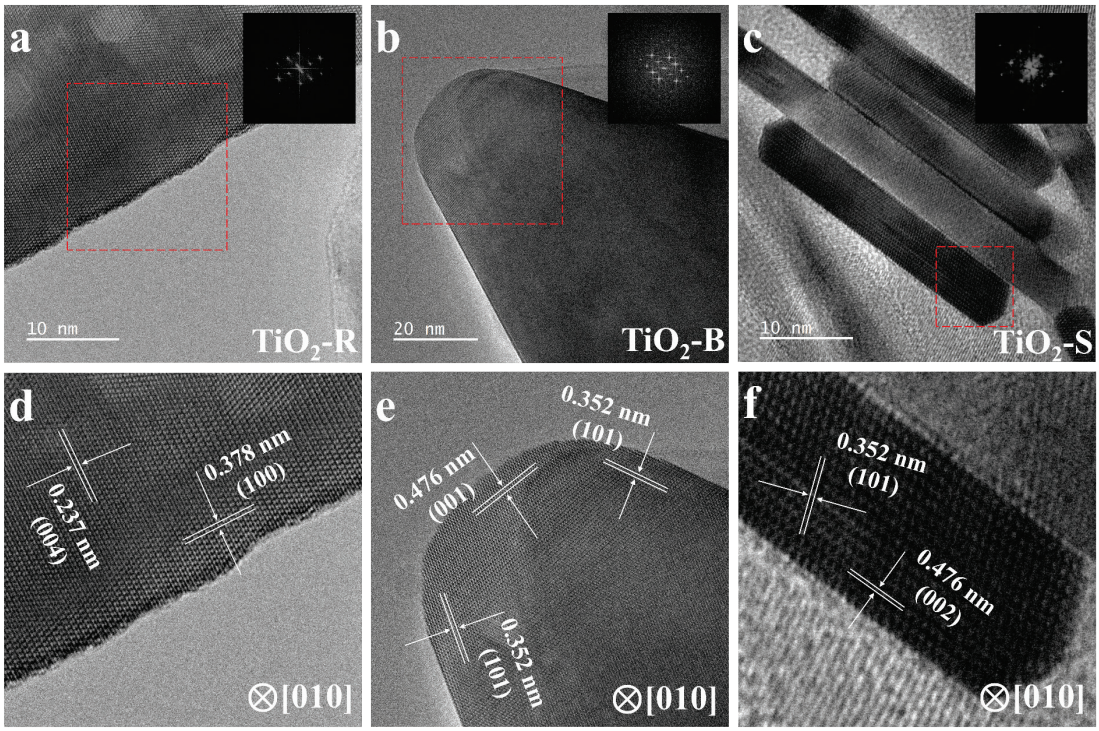

Supplementary Fig 1. *Ex-situ* Characterization of the TiO_2 supports. (a, d) TiO_2-R with (100) facet exposed; **(b, e)** TiO_2-B with (101) facet exposed; **(c, f)** TiO_2-S with (001) facet exposed.

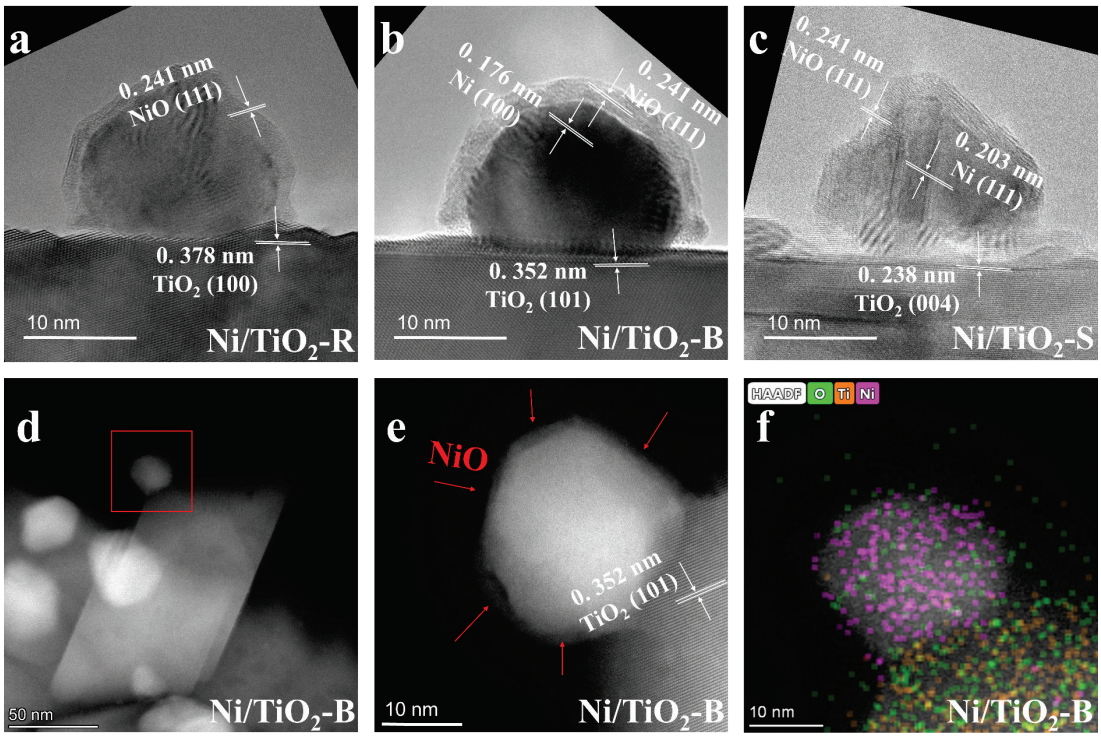

Supplementary Fig 2. *Ex-situ* Characterization of the Ni/TiO_2 catalysts. (a, b, c) HRTEM of three Ni/TiO_2 catalysts with NiO layer: Ni/TiO_2-R (a), Ni/TiO_2-B (b); Ni/TiO_2-S (c). **(d)** Low-magnification HAADF STEM image of Ni/TiO_2-B. **(e)** High-magnification images of the red regions in (d). **(f)** Elemental identification of the layer by EDX mapping of (e).

Supplementary Note 1: As shown in Supplementary Figs. 1a-c, three TiO_2 supports were all imaged along the [011] direction[1,2]. Similarly, the three Ni/TiO_2 catalysts were also observed along the [011] direction, where an overlayer surrounding the Ni NPs could be clearly identified. Based on the differences in lattice fringes, the outermost layer exhibited a larger lattice spacing (~0.24 nm), characteristic of NiO (Supplementary Figs. 2a-c). Furthermore, EDX analysis of the outermost layer revealed no detectable Ti signal, indicating that the surface layer was composed primarily of NiO (Supplementary Fig. 2f). This observation was consistent with previous reports, which show that Ni was readily oxidized upon exposure to air[3,4].

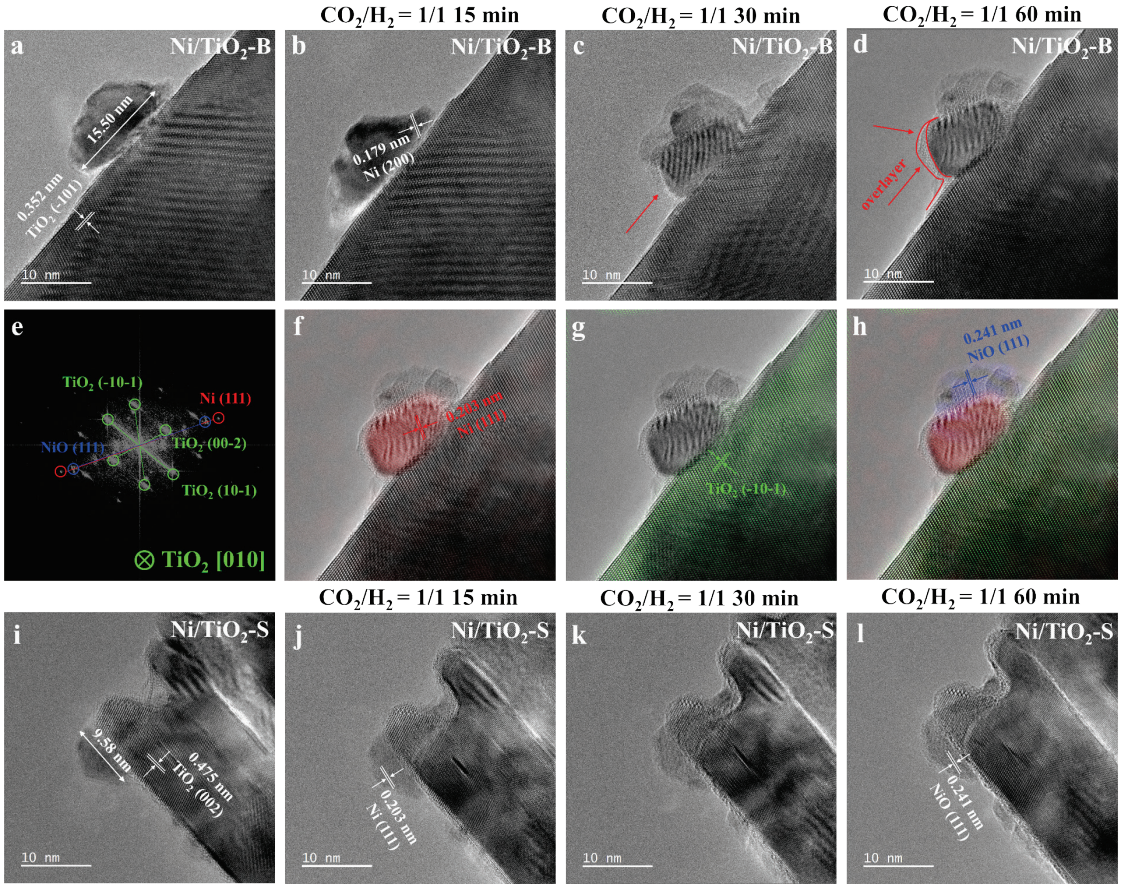

Supplementary Fig 3. The tunable Ni/TiO_2-B and Ni/TiO_2-S interface under different gas environments. *In-situ* ETEM images of Ni/TiO_2-B in **(a)** reducing atmosphere (H_2/N_2 = 10/90, 5×10^{-2} Pa, 400 °C), and **(b, c, d)** CO_2 hydrogenation conditions ($CO_2/H_2/N_2$ = 15/15/70, 5×10^{-2} Pa, 350 °C). **(e)** FFT patterns of the HRTEM images of Ni/TiO_2-B in (d). The FFT spots of Ni, NiO and TiO_2 are labeled by the red, blue and green dashed circles, respectively. **(f, g, h)** Inverse FFT analysis of three phases (Ni, TiO_2, NiO). *In-situ* ETEM images of Ni/TiO_2-S in **(i)** reducing atmosphere (H_2/N_2 = 10/90, 5×10^{-2} Pa, 400 °C), and **(j, k, l)** CO_2 hydrogenation conditions ($CO_2/H_2/N_2$ = 15/15/70, 5×10^{-2} Pa, 350 °C).

Supplementary Note 2: As shown in Supplementary Figs. 3a, i, the NiO overlayer was removed following H_2 treatment, exposing metallic Ni particles with representative sizes (~15.5 nm for Ni/TiO_2-B, ~9.6 nm for Ni/TiO_2-R), which were subsequently selected to monitor the structural evolution (Supplementary Figs. 3b-d and Figs. 3j-l). After 60 min of reactions, partial encapsulation was observed in Ni/TiO_2-B (Supplementary Fig. 3d), whereas no encapsulation layer formed in Ni/TiO_2-S (Supplementary Fig. 3l). Furthermore, the FFT patterns of the HRTEM images from Ni/TiO_2-B (Supplementary Fig. 3d) indicated that the overlayer could prevent Ni oxidation. In contrast, uncoated regions underwent phase transformation into NiO (Supplementary Figs. 3e-h). Similarly, the slight oxidation of Ni was observed on the Ni/TiO_2-S catalyst, as evidenced by the differences in lattice spacings (Supplementary Figs. 3j, l).

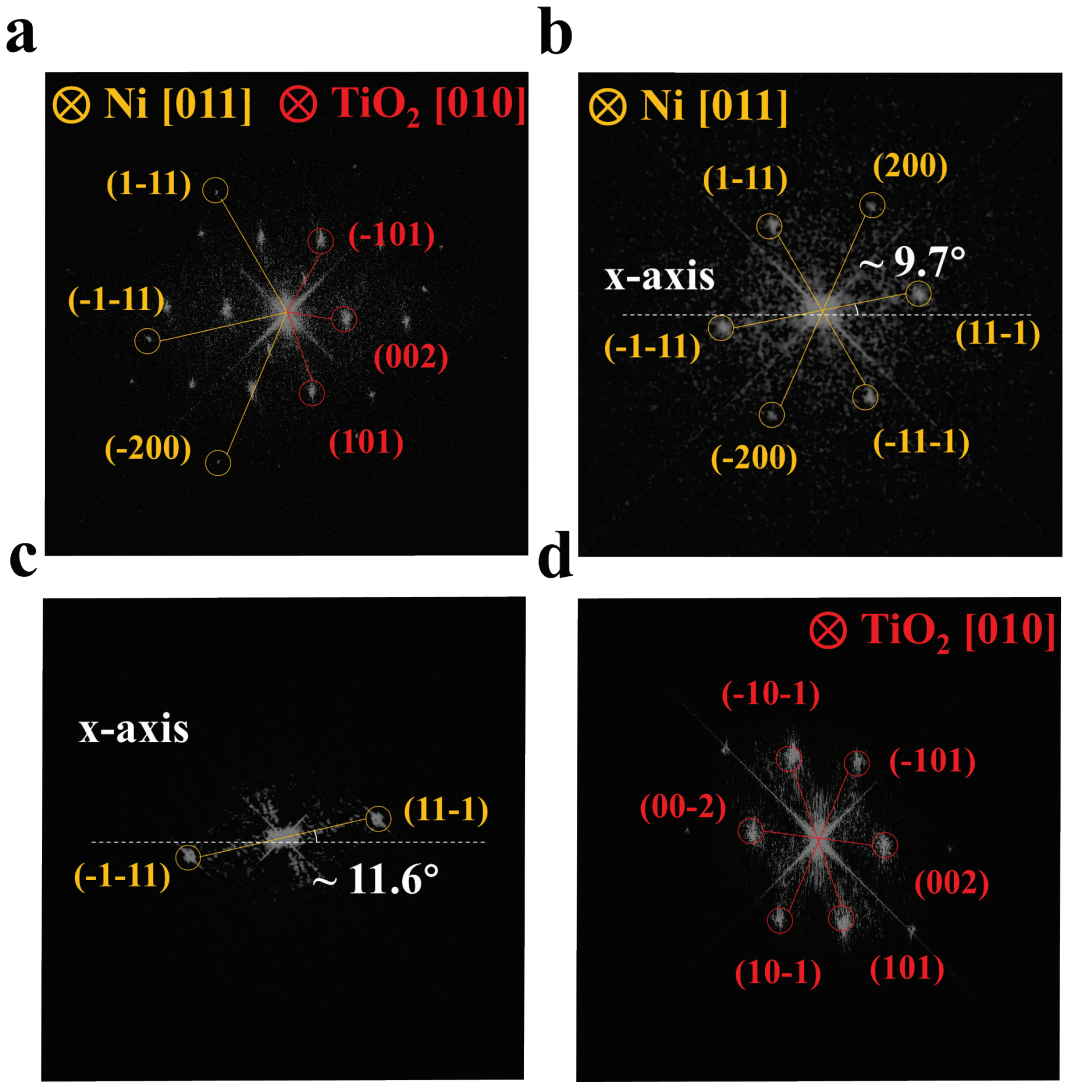

Supplementary Fig 4. FFT patterns of the HRTEM images of Ni/TiO_2-R in Figure 2. (a) FFT patterns of Fig. 2a. **(b)** FFT patterns of the boxed region in Fig. 2b. **(c)** FFT patterns of the boxed region in Fig. 2c. **(d)** FFT patterns of Fig. 2d.

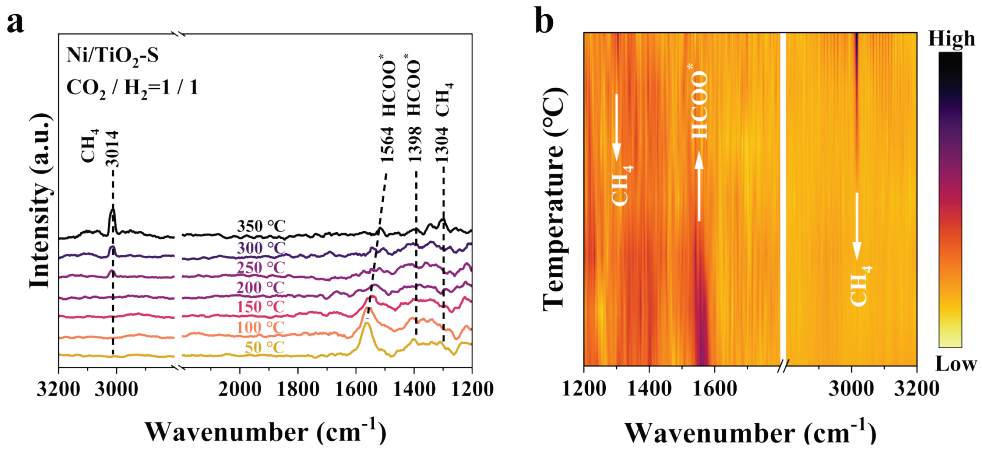

Supplementary Fig 5. **DRIFTS investigation of Ni/TiO_2-S catalysts. (a, b)** The spectra of Ni/TiO_2-S at different temperatures with a controlled heating rate of 10 °C/min. (CO_2/H_2/N_2 = 15/15/70). The sample was reduced under H_2 (H_2/N_2 = 10/90) at 400 ℃ to remove the NiO overlayer caused by exposing in air and then cooled in N_2 at 25 ℃ to obtain a background spectrum, afterwards reactive gas mixtures (CO_2/H_2/N_2 = 15/15/70) were introduced with a total flow rate of 100 mL/min.

Supplementary Note 3: The $HCOO^*$ intensity significantly diminished, accompanied by the emergence of characteristic CH_4 peaks. This indicates that $HCOO^*$ serves as a key intermediate for CH_4 formation on the Ni/TiO_2-S catalyst.[5]

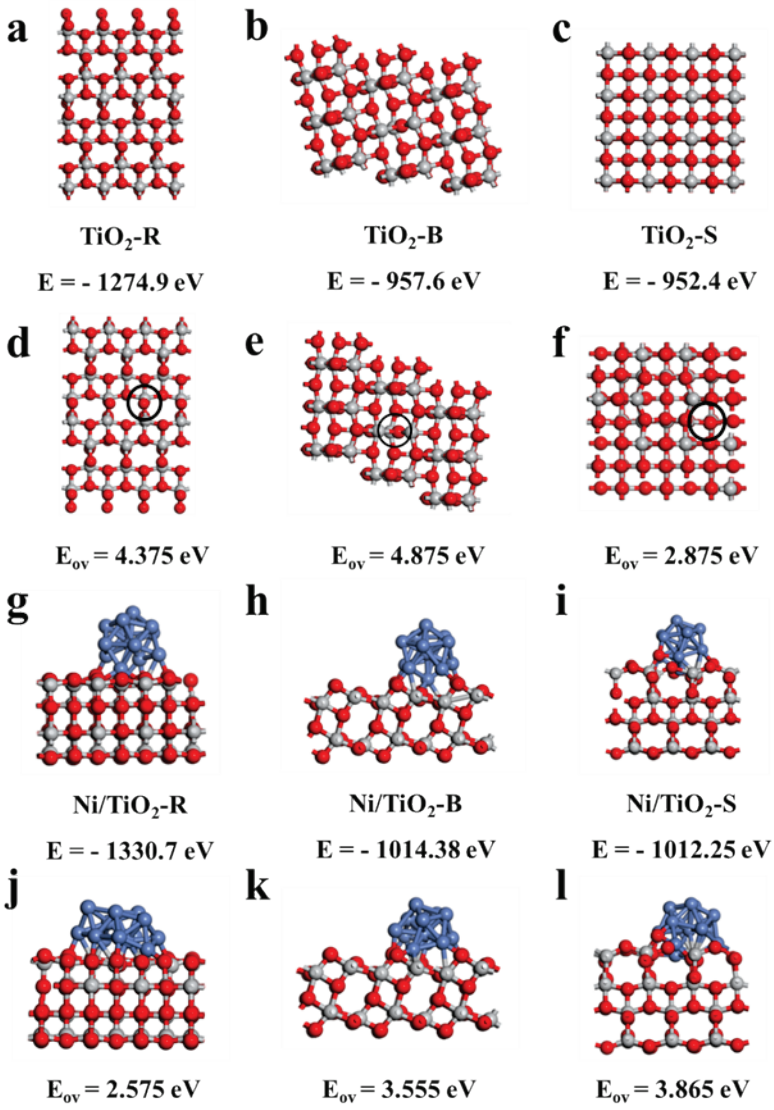

Supplementary Fig 6. **DFT calculation of various Ni/TiO_2 catalysts. (a, b, c)** The surface energy of Ni/TiO_2-R (a), Ni/TiO_2-B (b), and Ni/TiO_2-S (c). **(d, e, f)** The oxygen vacancy formation energy of Ni/TiO_2-R (d), Ni/TiO_2-B (e), and Ni/TiO_2-S (f). **(g, h, i)** The energy of Ni/TiO_2 system: Ni/TiO_2-R (g), Ni/TiO_2-B (h), and Ni/TiO_2-S (i). **(j, k, l)** The interface oxygen vacancy formation energy of Ni/TiO_2-R (j), Ni/TiO_2-B (k), and Ni/TiO_2-S (l).

Supplementary Note 4: Due to the differences in coordination environments of surface atoms on various TiO_2 crystal facets (Figs. 1d, e, f)[2], the formation energies of oxygen vacancies varied among the three supports, following the order: TiO_2-B (4.875 eV) > TiO_2-R (4.375 eV) > TiO_2-S (2.875 eV) (Supplementary Figs. 6a–f).[1,6] However, upon Ni loading, the oxygen vacancy formation energies at the Ni/TiO_2 interface changed significantly. Specifically, the formation energies decreased for Ni/TiO_2-R and Ni/TiO_2-B, but increased for Ni/TiO_2-S, resulting in a new trend: TiO_2-S (3.865 eV) > TiO_2-B (3.555 eV) > TiO_2-R (2.575 eV). These shifts provided for the facet-dependent nature of A-SMSI formation.

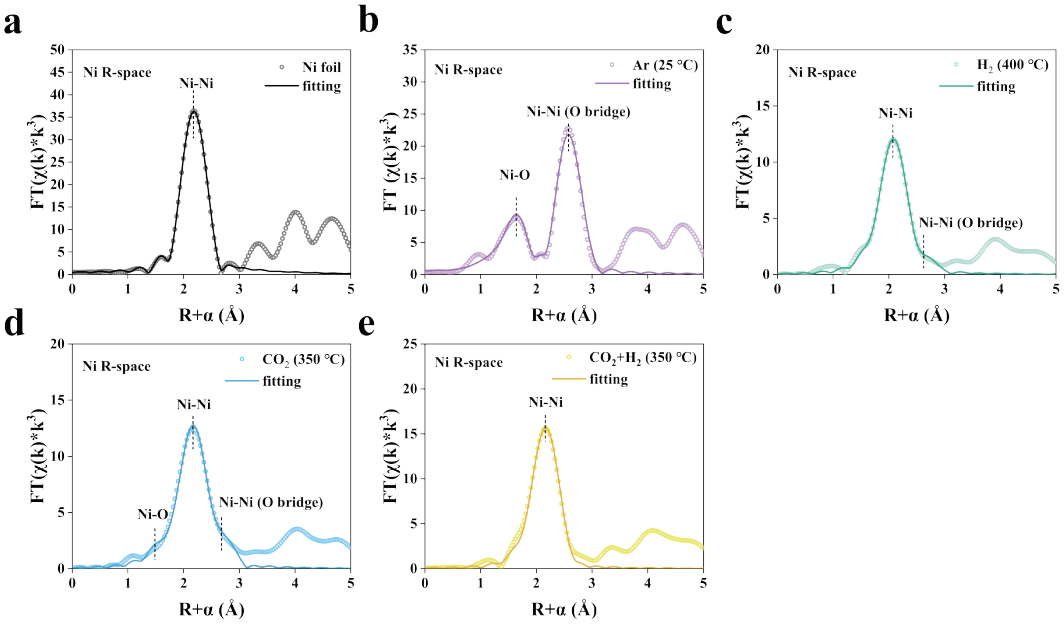

Supplementary Fig 7. Fourier transform EXAFS spectra and fitting of Ni/TiO_2-R catalysts. Fourier transform EXAFS spectra and fitting at Ni K-edge for **(a)** Ni foil; **(b)** NiO/TiO_2-R (25 °C, Ar); **(c)** Ni/TiO_2-R (400 °C, H_2); **(d)** Ni/TiO_2-R (350 °C, CO_2); **(e)** Ni/TiO_2-R (350 °C, CO_2 + H_2).

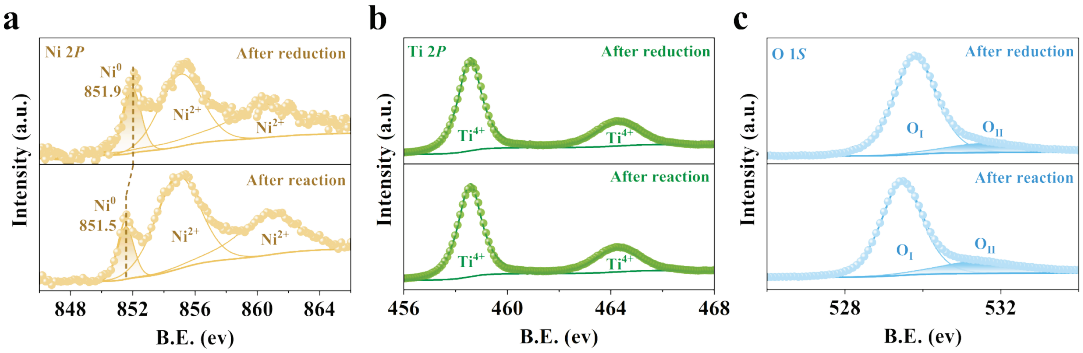

Supplementary Fig 8. XPS spectra of Ni/TiO_2-R catalyst. (a) Ni 2*p*, **(b)** Ti 2*p*, and **(c)** O 1*s*. The sample was analyzed after *ex-situ* reduction (400 ℃, H_2) and reaction (350 ℃, CO_2 + H_2).

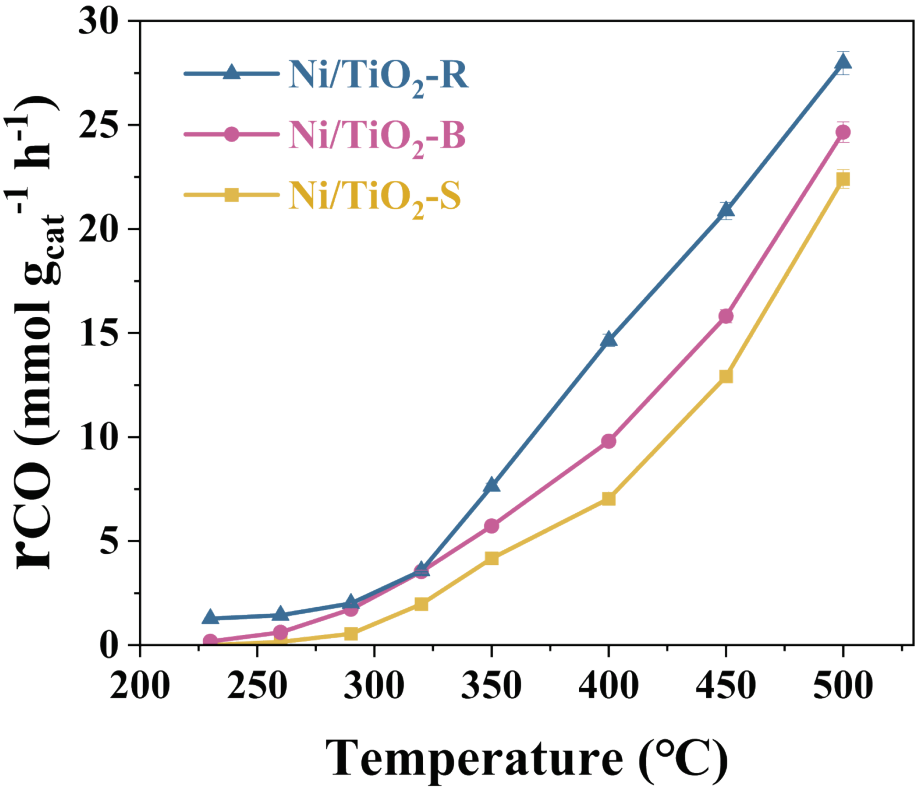

Supplementary Fig 9. CO production rate over various Ni/TiO_2 catalysts at a temperature range of 200-500 °C. Reaction conditions: catalysts (1000 mg), 1 bar, $CO_2/H_2/N_2$ = 15/15/70; GHSV: 12000 mL g cat^{-1} h^{-1}).

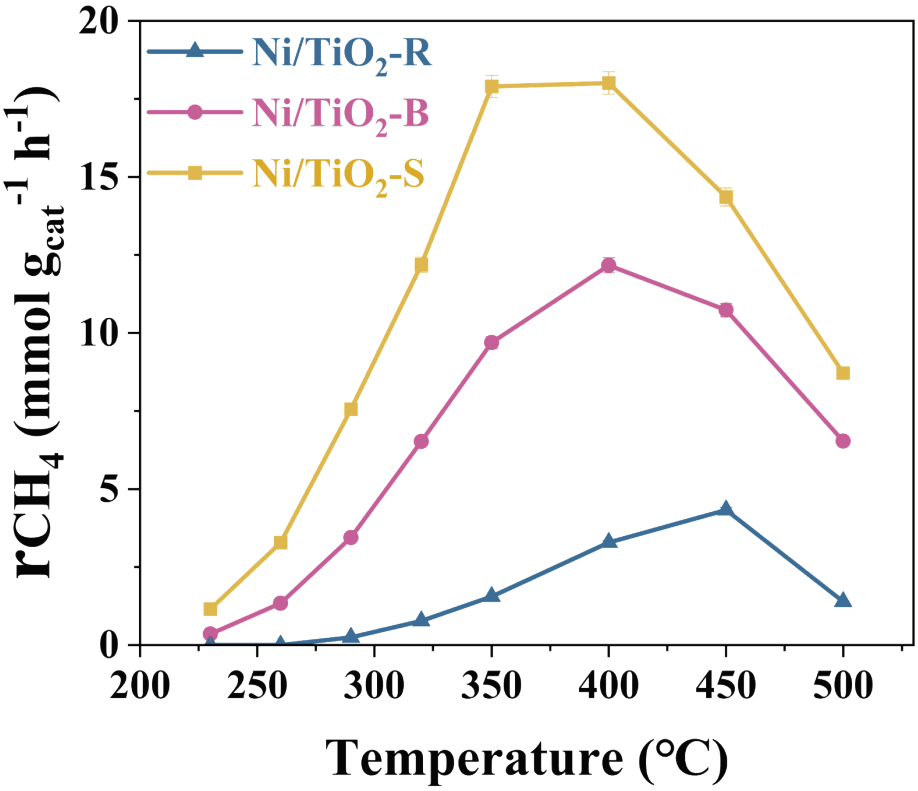

Supplementary Fig 10. CH_4 production rate over various Ni/TiO_2 catalysts at a temperature range of 200-500 °C. Reaction conditions: catalysts (1000 mg), 1 bar, $CO_2/H_2/N_2$ = 15/15/70; GHSV: 12000 mL g cat^{-1} h^{-1}).

Supplementary Table 1. EXAFS fitting parameters at the Ni K-edge for various Ni/TiO_2 catalysts at different conditions.

Sample	Condition	Shell	N [a]	R (Å) [b]	σ^2 [c] (Å^2·10^{-3})	R factor (%)
Ni foil	Air, 25 ℃	Ni−Ni (in metallic state Ni)	9.3±0.3	2.48±0.01	5.97±0.29	0.19
NiO/TiO_2-R	Ar, 25 ℃	Ni−O	6.0±0.2	2.09±0.01	8.0±2.2	0.72
		Ni−Ni (O-bridged)	11.8±0.2	2.95±0.01	9.1±1.2	
Ni/TiO_2-R	H_2, 400 ℃	Ni−Ni (in metallic state Ni)	6.6±0.7	2.46±0.01	11.2±0.9	0.47
	CO_2, 350 ℃	Ni−O	1.6±0.5	2.95±0.02	11.2±0.9	0.35
		Ni−Ni (in metallic state Ni)	6.0±0.7	2.47±0.01	10.8±1.1	
		Ni−O	1.1±0.2	2.02±0.01	7.0±4.7	
		Ni−Ni (O-bridged)	2.3±1.0	2.96±0.01	10.5±4.5	
	CO_2+H_2, 350 ℃	Ni−Ni (in metallic state Ni)	8.6±0.7	2.48±0.01	11.6±0.9	0.98

a N: coordination number; **b R:** bond distance; **c σ^2:** Debye-Waller factor; **R factor:** goodness of fit.

Supplementary References

1. Li, S. *et al.* Unusual Facet-Dependent Sintering in Pd–TiO_2 Catalysts Revealed by Theory and Experiment. *ACS Catal.* **14**, 1608–1619 (2024).

2. Tang, M. *et al.* Facet-Dependent Oxidative Strong Metal-Support Interactions of Palladium–TiO_2 Determined by In Situ Transmission Electron Microscopy. *Angew Chem Int Ed* **60**, 22339–22344 (2021).

3. Xu, M. *et al.* Boosting CO hydrogenation towards C_{2+} hydrocarbons over interfacial TiO_{2-x}/Ni catalysts. *Nat Commun* **13**, 6720 (2022).

4. Cui, B. *et al*. Crystal-phase-depended strong metal-support interactions enhancing hydrodeoxygenation of m-cresol on Ni/TiO_2 catalysts. *Journal of Catalysis* **413**, 880–890 (2022).

5. Tan, T. H. *et al.* Unlocking the potential of the formate pathway in the photo-assisted Sabatier reaction. *Nat Catal* **3**, 1034–1043 (2020).

6. Wu, Y. *et al.* Study of Oxygen Vacancies on Different Facets of Anatase TiO_2. *Chin. J. Chem.* **37**, 922–928 (2019).